Quantum Electronics **52** (2) 160–170 (2022)

BIOPHOTONICS

https://doi.org/10.1070/QEL17984

Laser fragmentation of silicon microparticles in liquids for solution of biophotonics problems

V.Yu. Nesterov, O.I. Sokolovskaya, L.A. Golovan, D.V. Shuleiko, A.V. Kolchin, D.E. Presnov, P.K. Kashkarov, A.V. Khilov, D.A. Kurakina, M.Yu. Kirillin, E.A. Sergeeva, S.V. Zabotnov

Abstract. **The possibility of manufacturing silicon nanoparticles by picosecond laser fragmentation of silicon microparticles in water is analysed. It is shown that for fragmentation duration of 40 min, the dependence of the average sizes of particles on the initial mass concentration of the micropowder varied in the range of 0.5–12 mg mL^{-1} is nonmonotonic, with the maximum average size of 165 nm being achieved at a concentration of 5 mg mL^{-1}. To explain the obtained result, the simulation of propagation of a focused laser beam in a scattering suspension of silicon microparticles is performed for their different mass concentrations. It is demonstrated that at concentrations not exceeding 5 mg mL^{-1}, fragmentation occurs in the paraxial region of the beam when it propagates deep into the cuvette with a suspension, while at higher concentrations it occurs primarily in the superficial layer owing to strong extinction. Calculations results allow the experimental features of the formation of silicon nanoparticles to be explained. Spectrophotometry measurements on suspensions of nanoparticles obtained at the initial concentration of microparticles of 12 mg mL^{-1} are compared with the theoretical estimates of the absorption and scattering coefficients obtained in the framework of the Mie theory. Measured optical properties indicate the potential of using fragmented nanoparticles as scattering and/or absorbing contrast agents in optical imaging of biological objects.**

Keywords: *silicon micro- and nanoparticles, laser fragmentation in liquids, light scattering, Monte Carlo technique, spectrophotometry.*

V.Yu. Nesterov, O.I. Sokolovskaya, L.A. Golovan, D.V. Shuleiko, A.V. Kolchin, P.K. Kashkarov, S.V. Zabotnov Faculty of Physics, Lomonosov Moscow State University, Leninskie Gory 1, stroenie 2, 119991 Moscow, Russia; e-mail: zabotnov@physics.msu.ru;
D.E. Presnov Faculty of Physics, Lomonosov Moscow State University, Leninskie Gory 1, stroenie 2, 119991 Moscow, Russia; Skobeltsyn Institute of Nuclear Physics, Lomonosov Moscow State University, Leninskiye Gory 1, stroenie 2, 119991 Moscow, Russia; Center for Quantum Technologies, Lomonosov Moscow State University, Leninskie Gory 1, stroenie 35, 119991 Moscow, Russia;
A.V. Khilov, D.A. Kurakina Institute of Applied Physics, Russian Academy of Sciences, ul. Ulyanova 46, 603950 Nizhny Novgorod, Russia;
M.Yu. Kirillin Institute of Applied Physics, Russian Academy of Sciences, ul. Ulyanova 46, 603950 Nizhny Novgorod, Russia; Lobachevsky State University of Nizhny Novgorod, prosp. Gagarina 23, 603022 Nizhny Novgorod, Russia;
E.A. Sergeeva Institute of Applied Physics, Russian Academy of Sciences, ul. Ulyanova 46, 603950 Nizhny Novgorod, Russia; Faculty of Physics, Lomonosov Moscow State University, Leninskie Gory 1, stroenie 2, 119991 Moscow, Russia

Received Received 24 November 2021
Kvantovaya Elektronika **52** (2) 160–170 (2022)
Translated by M.Yu. Kirillin

1. Introduction

Progress in the use of silicon nanoparticles (SiNPs) in such biomedical applications as targeted drug delivery [1, 2], fluorescence imaging of biotissues [3, 4], ultrasound [4] and photodynamic [5–7] therapy, hyperthermia [8–10] and optical coherence tomography (OCT) [11] is inextricably linked with the ongoing development of nanostructuring technologies for this material. Electrochemical etching is a traditional approach to fabricating porous silicon layers that are subsequently mechanically or ultrasonically ground to produce SiNPs suitable for the abovementioned applications, because such SiNPs have a low degree of toxicity and a relatively fast degree of biodegradation in living organisms [1–4]. Besides porous silicon, arrays of silicon nanowires can also be used as a nanostructured basis for the SiNP production [12, 13]. However, as a rule, in the listed cases, mechanical or ultrasonic grinding of porous matrices cannot be treated as an ultimate technological stage in terms of controlling particle size distributions in a wide range and does not allow one to avoid residual undesirable chemical impurities after chemical etching of silicon.

To a large extent, the method of pulsed laser ablation of silicon in various liquids is free of these drawbacks, while the choice of a proper liquid along with varying the parameters of laser irradiation allows fabricating SiNPs with desired size distributions in the range from a few to hundreds of nanometres with a high degree of chemical purity [14–16]. SiNPs formed using this approach can be used for fluorescence imaging of biological tissues [17], contrasting images in biotissue visualisation using optical coherence tomography [11, 16, 18], in photodynamic therapy [19], tissue engineering [20], and photohyperthermia [21, 22]. A significant disadvantage of this approach is the requirement to use lasers for ablation that generate high-power pulses with a high repetition rate in order to ensure the fabrication of SiNPs at concentrations sufficient for use in the mentioned applications. Nevertheless, the requirements to a laser source can be reduced by using preliminarily nanostructured porous targets with a reduced ablation threshold compared to crystalline silicon. Layers of porous silicon [23] or arrays of silicon nanowires [24] can serve as such targets. The SiNPs formed using this approach are of undoubted interest for biophotonics due to their fluorescence properties and efficient light scattering in the diagnostic transparency window of biological tissues [16, 25].

Laser fragmentation of silicon preliminarily mechanically ground into particles of micron or submicron sizes in liquids is a simpler, but yet effective technology from the point of view of SiNP production. In this case, in the absence of any chemical processing of silicon in the ablation in a sufficiently

large volume of a suspension, in contrast to a planar target, allows fabricating ensembles of nanoparticles with relatively narrow size distributions [26, 27] and a high degree of crystallinity [28]. Currently, there is every reason to believe that the sizes of the fabricated SiNPs depend on the initial concentration of silicon in suspension. However, the results obtained earlier show both an increase in the average SiNP size with increasing concentration [26, 27], and vice versa [29]. It is important to note that these works present only empirical dependences of the sizes of fragmented SiNPs on the concentration without a detailed theoretical substantiation of the results obtained. Moreover, in previous studies, the initial concentration of silicon microparticles was limited to 1 mg mL^{-1}. Therefore, further studies are required, taking into account the features of the propagation and focusing of a high-power laser beam in suspensions of silicon microparticles (SiMPs) with various concentrations, including relatively high ones. An additional study of light scattering and absorption of already fragmented SiNPs is also needed in order to assess the prospects for their further use as contrast agents in problems of visualisation of biological objects.

In this work, SiNP suspensions were fabricated by picosecond fragmentation of SiMPs in water with varying the initial concentration of irradiated microparticles in the range from 0.5 to 12 mg mL^{-1}, and numerical simulation of the process of laser pulse propagation in such media and absorption-induced heating and melt of microparticles was performed. The simulation of radiation propagation in the medium was performed by the Monte Carlo technique, while the calculation of temperature maps was carried out using the local application of the heat balance equation. Based on spectrophotometric data in the wavelength range of 400–1000 nm, we analysed the spectra of the elastic scattering and absorption coefficients for the SiNP suspension produced by laser fragmentation of SiMPs with a concentration of 12 mg mL^{-1}. The mass outcome for fragmentation products and further potential of such nanosystems for contrasting biotissues were estimated.

2. Materials and methods

2.1. Samples under study and experimental techniques

For SiNP fabrication, the SiMPs with a size of 1–8 μm (Fig. 1) produced by mechanical grinding of crystalline chemically pure (99.99%) silicon (Plazmaterm Ltd, Russia) were used as targets for laser fragmentation.

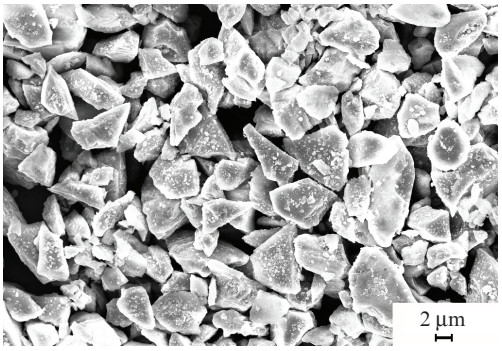

Figure 1. SEM image of the initial powder of microcrystalline silicon.

Fragmentation was performed in fixed glass cuvettes with a base of 10×10 mm, filled to a height of 10 mm with suspensions of the SiMPs with various mass concentrations C in distilled water (Table 1). The mass of the dry micropowder before being suspended in water was measured by the gravimetric method. Immediately before fragmentation, the suspension in the cuvette was homogenised using an ultrasonic bath.

Table 1. Parameters of SiNP fabrication by laser fragmentation of SiMP suspensions in distilled water.

Fragmentation time/min	Initial SiMP concentration/ mg mL^{-1}	Average SiNP size/nm	Standard deviation/nm
	0.5	134	49
	1.8	149	60
40	5.0	165	76
	7.0	146	51
	12.0	147	56
90	5.0	111	48

The impact on the water suspension of SiMPs was performed using the radiation of a picosecond Nd:YAG laser EKSPLA PL2143A (Lithuania) (wavelength of 1064 nm, duration of 34 ps, energy of 16 mJ and pulse repetition rate of 10 Hz). The fragmentation time was 40 or 90 min (Table 1). Radiation was injected using a fixed system of mirrors through the open upper part of the cell normal to its base by focusing the Gaussian beam by a lens with a focal length $f_l = 80$ mm to the centre of the irradiated suspension, corresponding to a depth of $z_f = 5$ mm from the liquid surface. The laser beam radius on the water surface was estimated as $r = r_0 z_f / f_l = 0.25$ mm, where $r_0 = 4.0$ mm is the beam radius at the laser output.

The use of water as a buffer medium, on the one hand, allows relatively stable SiNP ensembles to be formed in the ablation regime [23–26], and, on the other hand, suggests further use of the produced SiNP suspensions directly in experiments with biological tissues and their phantoms due to the compatibility of this fluid with living organisms.

Separation of SiMPs that did not undergo fragmentation was carried out by sedimentation in prepared suspensions using an Eppendorf centrifuge 5424 (Germany) for 2 min at 3000 rpm and 7 min at 14000 rpm.

To study the structural properties of SiNPs, droplets of the fabricated suspensions were deposited on silicon or glass substrates. After drying, SiNPs on the substrates of the first type were analysed by scanning electron microscopy (SEM) using a Carl Zeiss Supra 40 (Germany) electron microscope; while for the SiNPs on the substrates of the second type Raman spectra were measured using a Horiba Jobin Yvon HR 800 (France) microscope with a probing He–Ne laser at a wavelength of 633 nm and a maximum power of 3 mW. Size distribution histograms of fabricated SiNPs were constructed based on the obtained SEM images. The sample size for constructing each histogram was 200–1000 particles. The values of the electrokinetic potentials (ζ-potentials) of SiNPs in suspensions were measured using a Malvern Zetasizer NANO-ZS analyser (UK).

The analysis of light scattering and absorption characteristics in the studied SiNP suspensions in water was carried out by measuring their collimated and diffuse transmission spec-

tra, as well as diffuse reflection spectra in the wavelength range of 400–1000 nm using an Analytik Jena SPECORD 250 spectrophotometer equipped with an integrating sphere. Suspensions were placed in quartz cells with a distance of 1 mm between the walls and were ultrasonicated immediately prior to measurements to eliminate possible agglomeration and sedimentation of SiNPs in suspensions. Reconstruction of the scattering coefficient μ_s, absorption coefficient μ_a, and anisotropy factor $g = \langle\cos\theta\rangle$ (θ is the scattering angle) was performed based on the spectrophotometric data using the inverse Monte Carlo method described in detail in [25]. The final spectra of the SiNP absorption coefficient are given after subtracting the contribution of water absorption in the studied wavelength range. To analyse the fractional content of particles in the final suspension, the measured spectra of the absorption and scattering coefficients were compared with the SiNP spectra calculated using the Mie formulae based on the histograms of the SiNP size distribution obtained by the SEM technique, in which the possible insignificant presence of a fraction of the initial SiMPs was taken into account as spherical particles of 5 μm in diameter. According to the best fit between the reconstructed and calculated spectra, two parameters were determined: the percentage of the SiMP fraction and the total mass concentration of SiMPs and SiNPs in the final suspension. The obtained parameters were used to estimate the mass concentration of SiNPs with sizes below 500 nm, which allows one to estimate the useful yield of laser fragmentation products.

2.2. Numerical simulation of focused laser beam propagation in an aqueous suspension of SiMPs and its heating

To understand the processes occurring during laser irradiation of a SiMP suspension, it seems reasonable to estimate the temperatures reached by SiMPs and the probabilities of phase transitions in them. It should be taken into account that the establishment of equilibrium between the electronic and lattice subsystems occurs at times much shorter than the duration of the employed laser pulse [30, 31]. At the same time, during the laser pulse impact the diffusion of heat is insignificant and can be omitted in estimation of the maximum temperatures reached by SiMPs during irradiation. During the period between consequent laser pulses, the suspension cools down almost completely, and, in this connection, consideration of the absorption of the energy of a single laser pulse is sufficient for simulations.

The energy distribution of a single laser pulse absorbed by SiMPs and their temperatures reached were estimated using the Monte Carlo technique [32–34] for a single laser pulse with the characteristics listed above. The total considered volume is $L_xL_yL_z = 4 \times 4 \times 7.8$ mm, in which, according to visual observations with an infrared imager, the most intensive interaction of radiation with SiMPs suspension occurs. The computational grid for the energy absorbed by silicon and its temperature in water suspension was an array of rectangular voxels with dimensions of $v = \Delta x\Delta y\Delta z = 0.01 \times 0.01 \times 0.03$ mm. The grid size was governed by the choice of sufficiently large (on the order of several units) values of ratios $2r/\Delta x$ and $b/\Delta z$, where b is the confocal parameter.

To simulate the propagation of a Gaussian beam with given focusing parameters, a quasi-optical approximation was employed. The coordinate system was chosen in such a way that the origin of coordinates is placed on the suspension surface, and the z axis is directed along the beam axis into the medium. The initial coordinates x_0, y_0 of each photon at the boundary plane ($z = 0$) were set using the Box–Muller transformation [35]:

$$x_0 = \xi_1\frac{r}{\sqrt{2}}, \quad y_0 = \xi_2\frac{r}{\sqrt{2}}, \tag{1}$$

where ξ_1 and ξ_2 are random values distributed according to the Gaussian law with $M = 0$ and $\sigma = 1$. The initial direction vector of the photon velocity was set in the direction of the focal point, which corresponds to the formation of the focus in the geometrical optics approximation. Since the selected size of the voxel exceeds the beam waist radius $r_f = f_1\lambda/(\pi r_0) = 0.0034$ mm, this simplification of the angular distribution does not distort the beam profile, since it adequately describes its shape outside the waist.

For a wavelength of 1064 nm, the imaginary part of the crystalline silicon refraction index has a strong dependence on temperature [36]:

$$\kappa(T) = \frac{\lambda}{4\pi}[12.991\exp(0.0048T) - 52.588\exp(-0.000226T)], \tag{2}$$

while its real part depends on temperature as [37, 38]

$$n(T) = 3.554 + 2.7 \times 10^{-4}T. \tag{3}$$

For molten silicon and the considered wavelength, the real and imaginary parts of the refractive index are $n = 5$ and $k = 6.8$, respectively [39]. The refractive indices n of water and water vapour equal 1.32 and 1.00, respectively [40].

The optical properties of SiMP suspensions were calculated according to the Mie theory [41] in the model approximation of silicon spheres of 5 μm in diameter. Despite the fact that real particles have an irregular polyhedral shape and a polydisperse size distribution due to the peculiarities of mechanical grinding (Fig. 1), this approximation is justified both by the absence of a pronounced shape anisotropy [42, 43] and by the estimate of the average size of SiMPs (as 5 μm) without ability for extraction of an accurate size distribution of such particles. The probability of photon scattering at the polar angle θ was determined by the Henyey–Greenstein phase function [44]:

$$p(\theta) = \frac{1}{4\pi}\frac{1-g^2}{(1+g^2-2g\cos\theta)^{3/2}}. \tag{4}$$

Table 2 shows the variation ranges of the scattering and absorption cross sections σ_s^{SMP} and σ_a^{SMP}, as well as the mean cosine of the scattering angle (anisotropy factor) g^{SMP} of a single SiMP for temperatures in the range from room temperature $T_0 = 300$ K to the melting temperature of silicon $T_m = 1687$ K, and from T_m to silicon evaporation temperature $T_{ev} = 3473$ K [45]. The scattering cross section of a single SiMP in the water suspension weakly depends on temperature, while its absorption cross section increases significantly with increasing temperature.

The absorption coefficient of radiation by water is $\mu_a^{wat} = 0.15$ cm^{-1}, while in the simulation the phase transition of water into water vapour was taken into account, as a result of which the medium surrounding SiMPs becomes nonabsorbing [46]. It is assumed in the calculations that the volume fraction of SiMPs in suspension is small, and the scattering and

Table 2. Variation ranges of the scattering and absorption cross sections, as well as the anisotropy factor of a single SiMP in the considered temperature ranges calculated using Mie theory.

Phase state	Temperature range/K	Scattering parameters		
		$\sigma_s^{SMP}/\mu m^2$	$\sigma_a^{SMP}/\mu m^2$	g^{SMP}
Crystalline silicon in water and water vapour	300–1687	28.63–45.49	0.096–15.95	0.47–0.74
Molten silicon in water vapour	1687–3473	37.23	7.08	0.58

absorption coefficients can be considered as additive quantities [47]:

$$\mu_a^{susp} = \mu_a^{wat} + \sigma_a^{SMP} N, \quad (5)$$

$$\mu_s^{susp} = \sigma_s^{SMP} N, \quad (6)$$

$$\mu_t^{susp} = \mu_s^{susp} + \mu_a^{susp}, \quad (7)$$

$$g^{susp} = g^{SMP}, \quad (8)$$

where N is the concentration of particles in the suspension, related with the mass concentration C of SiMPs in the suspension as

$$C = \tfrac{1}{6}\rho\pi d^3 N. \quad (9)$$

Table 3 presents the physical and optical properties of the considered SiMP suspensions used in the calculations. For the scattering and absorption coefficients, the ranges of their variation for temperature varying from T_0 to T_{ev} are indicated.

Thus, the simulations of the propagation of a single picosecond pulse of fragmenting laser radiation in a SiMP suspension requires simultaneous assessment of the absorbed energy and local temperature distributions. Therefore, the calculation was an iterative procedure consisting of the successive calculation of the distribution of the absorbed light energy in the medium and the heating of the medium caused by this absorption [48]. To account for the temperature dependence of the absorption of a laser pulse by silicon in a suspension, the calculation of the propagation of an initial pulse with an energy of 16 mJ consisted of 20 successive stages. The optical properties of the medium, μ_s^{susp}, μ_a^{susp}, and g^{susp}, within each voxel of the computational grid were considered constant. For each stage consisting of successive calculation of absorption and temperature maps in the SiMP suspension, simulations were performed for 10^7 photons.

At the calculation of the ith stage, the total energy absorbed during i stages by the silicon mass $m_v = Cv$ located within a single voxel of volume v is a discrete function $\Delta H(x,y,z,i)$, where x, y, and z are coordinates of the voxel centre. The energy absorbed by silicon in one voxel, $\Delta H(x,y,z,i)$, was converted into its temperature $T_i(x,y,z)$ for each voxel (x,y,z) by solving the heat balance equation for silicon mass m_v:

$$\Delta H(x,y,z,i) = \Delta H(x,y,z,i-1) + c_{Si}\, T_{i-1}(x,y,z)\, m_v [T_i(x,y,z) - T_{i-1}(x,y,z)], \quad (10)$$

where c_{Si} is the temperature-dependent heat capacity of silicon ($c_{Si} = c_{Si}^{(1)} = 0.7$ J g^{-1} and $c_{Si} = c_{Si}^{(2)} = 1$ J g^{-1} for temperatures below and above $T_a = 1373$ K, respectively) [45]; and $T_i(x,y,z)$ and $T_{i-1}(x,y,z)$ are the temperatures in the voxel at stages i and $i-1$, respectively.

Phase transitions were carefully taken into account by comparing the value of $\Delta H(x,y,z,i)$ at each stage with thresholds ΔH_{m1}, ΔH_{m2}, and ΔH_{ev1}, required for heating the silicon with mass m_v to the melting temperature, to completely melt it, and to heat silicon melt to the evaporation temperature, respectively. To calculate these heats, the following formulae were employed

$$\Delta H_{m1} = c_{Si}^{(1)} m_v (T_a - T_0) + c_{Si}^{(2)} m_v (T_m - T_a), \quad (11)$$

$$\Delta H_{m2} = \Delta H_{m1} + q_m m_v, \quad (12)$$

$$\Delta H_{ev} = \Delta H_{m2} + c_{Si}^{(2)} m_v (T_{ev} - T_m), \quad (13)$$

where q_m is the specific heat of silicon melting equal to 1.8 kJ (g °C)$^{-1}$ [49].

Thus, the silicon temperature distribution map $T(x,y,z)$ was obtained in a suspension irradiated by a single laser pulse.

3. Results and discussion

3.1. Size distributions of nanoparticles fabricated in different regimes of laser fragmentation

According to the SEM data, all fragmented SiNPs are quite smooth and have a shape close to spherical one (Fig. 2a) and a polydisperse size distribution. The smooth shape and spherical symmetry can be explained, as will be shown below, by the transition of silicon to a molten droplet-like state upon

Table 3. Physical and optical characteristics of SiMP suspensions used in the simulation.

SiNP mass concentration C/mg mL^{-1}	SiNM volume fraction f	Concentration N/cm^{-3}	μ_s^{susp}/mm^{-1}	μ_a^{susp}/mm^{-1}
0.5	2.15×10^{-4}	3.28×10^6	0.094–0.149	0.015–0.052
1.8	7.73×10^{-4}	1.18×10^7	0.338–0.537	0.016–0.188
5	0.0022	3.28×10^7	0.939–1.492	0.018–0.523
7	0.0030	4.59×10^7	1.314–2.088	0.019–0.732
12	0.0052	7.87×10^7	2.253–3.580	0.023–1.255

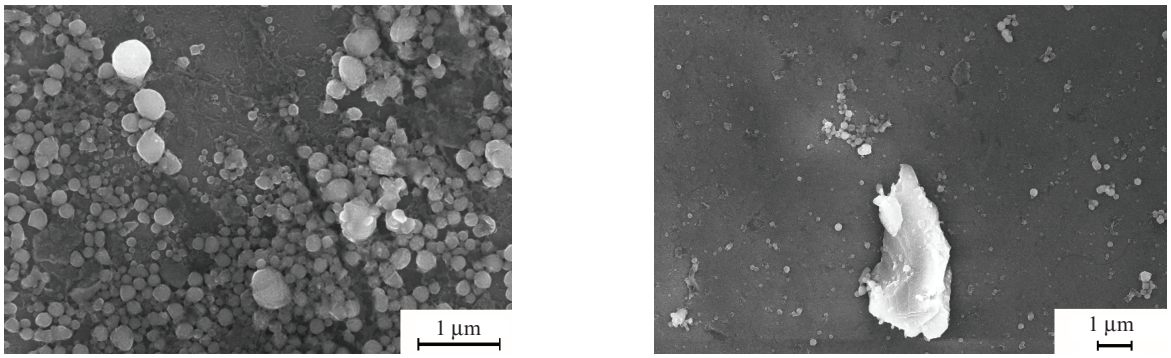

Figure 2. SEM images at (a) higher and (b) lower magnification of different areas of silicon substrates, where silicon particles were deposited after laser fragmentation of SiMPs with a mass concentration of 5 mg mL^{-1} for 40 min and centrifuging.

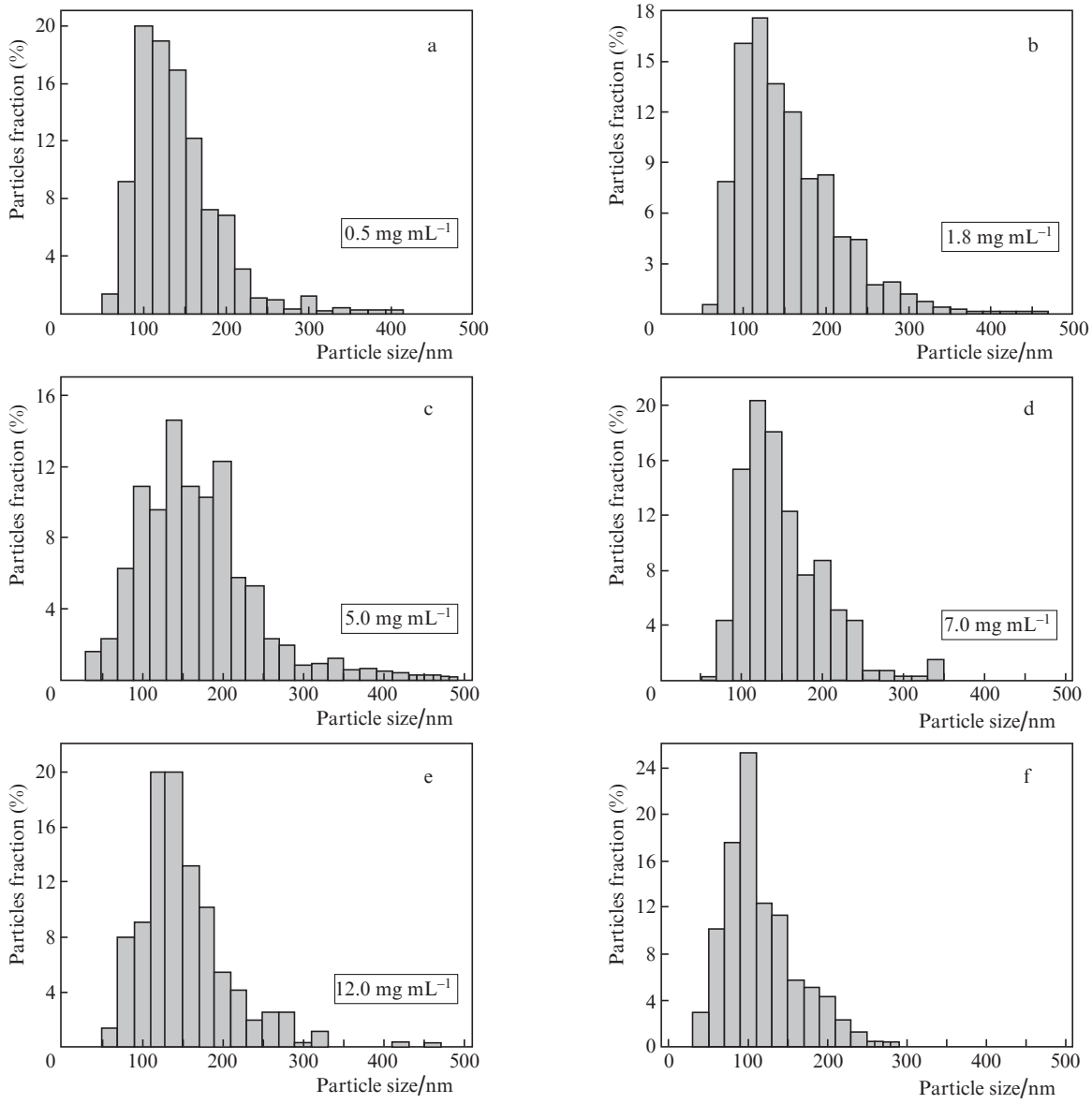

Figure 3. Size distribution histograms derived from SEM data for SiNPs produced by laser fragmentation in water of initial microcrystalline silicon powder with concentrations of (a) 0.5, (b) 1.8, (c) 5.0, (d) 7.0, and (e) 12.0 mg mL^{-1} for 40 min and (f) with initial concentration of 5.0 mg mL^{-1}for 90 min.

heating above the melting point of this material T_m = 1687 K as a result of laser fragmentation followed by cooling in a buffer liquid.

It is worth noting that, in addition to fragmented SiNPs, even after centrifugation, an insignificant (in number) fraction of microparticles that are not subjected to fragmentation (Fig. 2b) similar to the initial SiMPs (Fig. 1) remains in the suspension. The presence of this fraction indicates, firstly, a relatively low yield of the fragmentation product under the conditions of the experiment, and secondly, the probable diffusion of sedimented SiMPs into the region with SiNPs due to Brownian motion and spatial fluctuations in the distribution of this fraction within the cuvette volume under conditions of a real experiment. In the future, for further practical applications, the solution of the first problem can be found in the use of a laser source with higher repetition rates and pulse energies for fragmentation, while for the second problem a solution can be found in additional filtration of the resulting suspension using membrane filters. As part of this study, based on the approximation of spectrophotometric data, we estimate the ratio of the concentrations and mass contents of SiNPs and SiMPs remaining in suspension (see Section 3.3).

Since SiNP sizes no larger than 500 nm ensure efficient penetration of SiNPs into the body and their subsequent biodegradation and excretion [1, 3], the resulting fraction of fragmented particles is most interesting for biophotonics applications. SEM histograms of the size distributions of such SiNPs in all considered samples are shown in Fig. 3.

Polydisperse size distributions characterised by standard deviation values in the range from 48 nm to 76 nm (Table 1) are due to the formation of particle agglomerates of various sizes on different time scales at high temperature and pressure gradients in a medium irradiated by high-power laser pulses [50]. The average sizes and standard deviations of the produced SiNPs depend both on the initial mass concentration of SiMPs (Figs 3a–3e) and on the fragmentation time (Figs 3c, 3f). In the latter case, a noticeable decrease in both the average size from 165 nm to 111 nm and the standard deviation from 76 nm to 48 nm with an increase in the irradiation time to 90 min is associated with a larger number of interactions between laser radiation and SiMPs, secondary fragmentation of the already formed SiNPs, and well agrees with the monotonic decrease in the particle diameter with increasing exposure previously observed in [26].

A nonmonotonic dependence of the SiNP average sizes on the initial concentration of SiMPs was recorded for the first time: at concentrations not exceeding 5 mg mL^{-1}, an increase in the average size from 134 nm (at a concentration of 0.5 mg mL^{-1}) to 165 nm is observed; at higher concentrations a decrease is observed most probably reaching saturation at a value of about 147 nm (Table 1). Nevertheless, it is worth noting that an increase in the average size of SiNPs with an increase in the mass concentration of the initial powder of microcrystalline silicon under similar conditions of laser fragmentation was observed earlier in a work by Yu.V.Ryabchikov [26] at $C \leqslant 1$ mg mL^{-1}, which is in good agreement with our results for low concentrations. The inverse trend for low SiNP concentrations was observed in another paper [29] by the same author, where the synthesis of silicon–gold hybrid nanostructures using laser radiation was studied. However, in the latter case, a direct comparison of the results is not correct due to different technology employed consisting of several stages, including laser ablation of planar targets, and the effect of laser radiation on a suspension of silicon and gold particles, which is different from pure silicon.

3.2. Effect of laser beam propagation regime on sizes of fragmented nanoparticles

To explain the dependence of the average sizes of the SiNPs on the mass concentration of the microparticles in water, the propagation of the focused laser beam was considered in details accounting for the peculiarities of light scattering and absorbing by the SiMPs.

According to the technique described in Section 2.2, light energy absorption maps were calculated for a focused laser beam corresponding to the experimental conditions. Figure 4 shows the depth dependences of the absorbed energy $\Delta H(0,0,z,i)$ on the axis of the beam at different calculation stages.

For a small initial SiMP concentration of 0.5 mg mL^{-1} (Fig. 4a), the pulse scattering by the SiMP suspension is weak, and therefore the focusing of radiation in the medium is preserved (absorption maximum is located at the depth of z_f = 5 mm). With the increase in concentration from 0.5 to 5 mg L^{-1} (Figs 4a–4c), the radiation focusing is weakening, since the extinction by a turbid medium increases with increasing concentrations of scattering centres together with the increase in the absorption of scattered radiation near the surface (see Table 3). At concentrations of 7.0 and 12.0 mg L^{-1} (Figs 4d, 4e) the focusing area of the laser pulse is blurred, and the effective absorption by the SiMP suspension, sufficient for melting silicon at these concentrations ($\Delta H \geqslant \Delta H_{m1}$) occurs near the surface in contrast to depths compared to the focus location z_f = 5 mm, and the growth of the concentration leads to an increase in peak absorption and to a shift of the area of higher absorption towards the suspension surface. The size of the region where the absorbed energy exceeds ΔH_{m1} has the largest axial size for the concentration of C = 0.5 mg mL^{-1} compared with higher SiMP concentrations in the initial suspension $\Delta H_{m1}(C)$, which is governed by an increased scattering due to an increase in the concentration of SiMPs in suspensions. It is worth noting that the trends described were also visually observed in the experiment on the heat glow of the fragmented areas in the suspension volume or the subsurface region, depending on the initial SiMP concentration.

Figure 5 shows the cross sections $T(x,0,z)$ (Figs 5a–5d) and profiles $T(0,0,z)$ (Fig. 5e) of the distribution of silicon temperatures in the studied suspensions after absorption of the energy of a single laser pulse. For all the considered SiMP concentrations, a region exists, where silicon turns into to the molten phase, which confirms the assumption from Section 3.1 on the reason for the smoothness of the SiNP shape and the possible mechanism of their formation. In the employed model the heat ΔH required for the heating of silicon to a fixed temperature increases with an increase in the volume fraction of silicon in the SiMP suspension; therefore, a decrease in the area of effective heating is observed with increasing the SiMP concentration in the suspension (see Fig. 4).

The absorption and temperature maps allow estimating the total energy absorbed by silicon in the suspension in the melt region and the mass of molten silicon as

$$m_m = V_m f \rho, \tag{14}$$

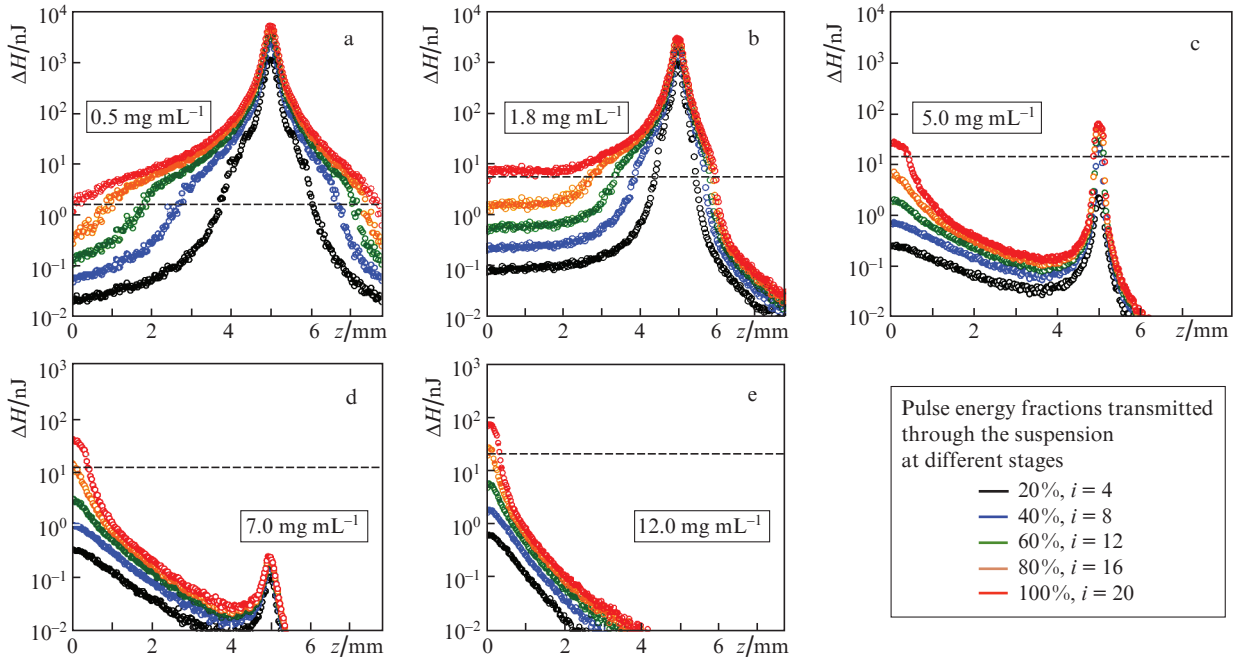

Figure 4. (Colour online) Profiles $\Delta H(0,0,z,i)$ of the energy absorbed by SiMPs contained in a single voxel on the axis of the beam in the aqueous suspension upon irradiation with a single laser pulse for the initial SiMP concentration of (a) 0.5, (b) 1.8, (c) 5.0, (d) 7.0, and (e) 12.0 mg mL^{-1}. Dashed lines show ΔH_{m1}.

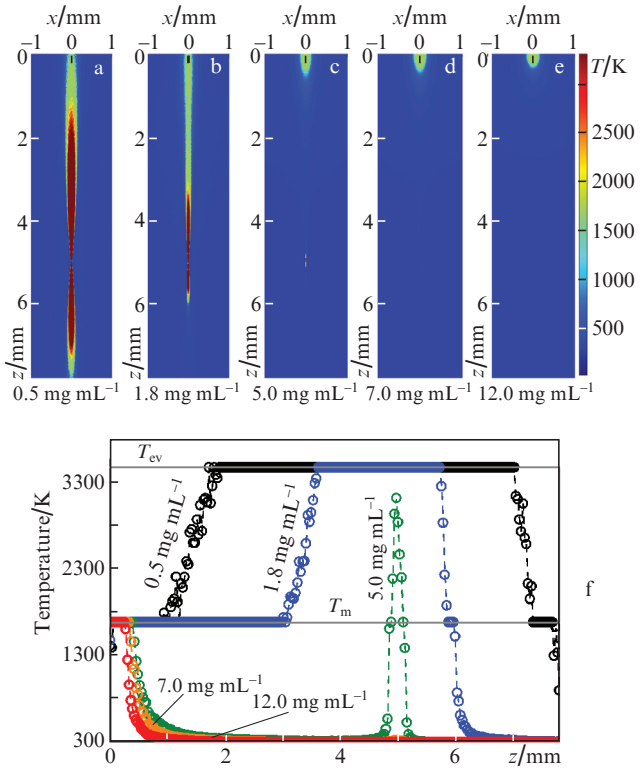

Figure 5. (Colour online) Cross sections $T(x,0,z,i=20)$ of temperature maps upon absorption of the energy of a single laser pulse by the SiMP suspension with initial concentrations of particles of (a) 0.5, (b) 1.8, (c) 5.0, (d) 7.0, and (e) 12.0 mg mL^{-1}; and (f) temperature profiles $T(0,0,z,i=20)$ on the beam axis for all considered concentrations.

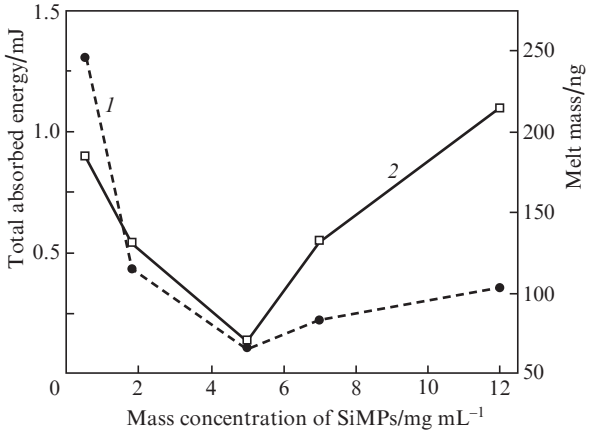

Figure 6. Dependence of the total energy absorbed by silicon in a suspension in the melt region (*1*) and the melt mass (*2*) produced during irradiation of the SiMP suspension with a single laser pulse with an energy of 16 mJ on the SiMP concentration in the suspension.

where V_m is the medium volume where the temperature T_m is reached, f is the volume fraction of silicon in the suspension, and $\rho = 2.33$ g cm^{-3} is the density of silicon [51]. The results of the estimates are presented in Fig. 6.

For SiMP concentrations below 5 mg mL^{-1}, absorption prevails in the region along the laser beam axis, while near the focus the silicon temperature significantly exceeds the melting temperature reaching the evaporation temperature in some regions (Fig. 5f). With an increase in the SiMP concentration to 5 mg mL^{-1}, the total absorbed energy in the molten silicon region and the mass of the melt (Fig. 6) decrease, because an increase in the concentration due to an increase in absorption and scattering results in a decrease in the intensity of the radiation reaching the beam focus. Nevertheless, the focused beam in the suspension for this concentration demonstrates a pronounced beam waist of a scale of a transverse size of a voxel $\Delta x = 0.01$ mm (Figs 5a–5c). When neglecting light scat-

tering effects, the waist diameter of the focused beam used in our experiments can be estimated as d_w = 0.014 mm [52]. Therefore, with a high accuracy, one can assume that at low mass concentrations of microparticles, their presence does not significantly affect the geometric characteristics of the beam waist affecting, however, suspension heating.

With a further increase in the SiMP concentration, the absorption of the laser pulse energy occurs mainly in the subsurface region, and the temperature of most SiMPs that have experienced a phase transition is close to the melting temperature (Figs 5c–5f). In this case, the energy absorbed by silicon and the mass of the melt increase (Fig. 6). One can assume that the indicated features of the interaction of a laser pulse with a SiMP suspension to some extent determine the size of the formed SiNPs. Thus, the smallest average SiNP diameter is achieved at a low concentration of SiMPs in the initial suspension and a noticeable overheating of silicon near the focus (Table 1). In the case of subsurface SiNP formation for SiMP concentrations above 5 mg mL^{-1}, when the silicon temperature slightly exceeds the melting point, the SiNP size is practically independent of the concentration. Finally, for a concentration of 5 mg mL^{-1}, when two SiNP generation centres exist in the suspension (in the focus and in the subsurface region) and the mass yield of SiNPs is lowered, the largest SiNP sizes and their greatest dispersion are achieved.

It is important to note that, despite a decrease in the fragmentation efficiency with an increase in the SiMP concentration, starting from 5 mg mL^{-1}, m_m increases due to the higher contribution of silicon volume fraction f in accordance to formula (14). It should be noted that the estimates of the mass of melted silicon per pulse shown in Fig. 6 are overestimated, and this overestimation is higher for cases of low concentrations of SiMPs. Thus, the absorption map was calculated for an effective medium, supposing that a particular amount of silicon that can absorb light energy is contained in each voxel of the medium. In reality, within that region consisting of several voxels the radiation is absorbed by a single microparticle, which can be located at a particular depth. The radiation reaching the microparticle can be attenuated due to absorption in the upper layers of the medium. The factor is especially important at the initial stages of pulse interaction with the medium for low SiMP concentrations.

This hypothesis is confirmed by the following estimates. Under the conditions of the experiment, the irradiation time of 40 min corresponds to N_{pulse} = 24000 laser pulses. Assuming that the fragmentation process was accompanied by permanent mixing of SiMPs in the area of laser beam impact due to their Brownian motion and probable convection and cavitation of water at high temperatures, the total mass of the SiNP yield as a result of fragmentation can be calculated as $N_{pulse} m_m$. In this case, for an initial SiMP concentrations of 0.5 and 12 mg mL^{-1}, the total mass yield of fragmented nanoparticles would be 4.4 and 5.2 mg, respectively, which corresponds to SiNP concentrations of 4.4 mg mL^{-1} and 5.2 mg mL^{-1}, assuming the volume of the fragmented suspension to be 1.0 mL. In the first case, the mass concentration of the fragmentation product exceeds the initial concentration of silicon in the suspension and, in the frames of the assumptions made, proves an overestimation of the calculated melt mass. It is vice versa in the second case for the maximum initial concentration of SiMPs, and this estimate seems to be more reasonable and close to reality. A more accurate estimate of the mass fraction of fragmented SiNPs will be given below based on the results of approximation of spectrophotometric data (see Section 3.3.2). Nevertheless, the analysis of the propagation and absorption of a laser beam in suspensions of SiMPs with different mass concentrations qualitatively confirms the undoubted influence of the focusing degree and radiation scattering on the size distribution of ragmented nanoparticles.

3.3. Optical properties of fragmented nanoparticles

3.3.1. Crystallinity and stability analysis. The high degree of crystallinity of the initial SiMPs is confirmed by the Raman spectroscopy data (Fig. 7a): In the range of 50–850 cm^{-1} their spectrum demonstrates a single line with a maximum at 521 cm^{-1}, which corresponds to the crystalline phase of silicon. The SiNPs after fragmentation and centrifugation also demonstrate similar spectra (see the example in Fig. 7b), which allows treating them as nanocrystals with a refractive index of 3.6–3.7 in the diagnostic transparency window of biotissues of 700–1300 nm [53]. The relatively high refractive index allows one to consider the SiNPs under study as effective light scatterers and, as a result, potential contrast agents in the OCT technique.

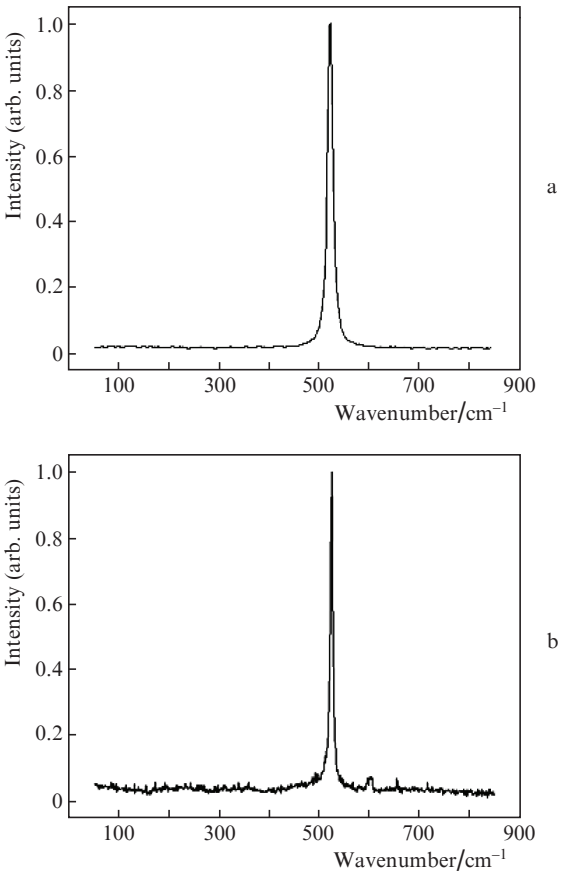

Figure 7. Raman spectra of (a) initial SiMPs and (b) SiNPs produced by laser fragmentation of SiMPs with a mass concentration of 5 mg mL^{-1} for 40 min in water. All spectra are normalised for the maximum Raman scattering intensity at 521 cm^{-1}.

The produced suspensions of SiNPs in water are characterised by absolute values of electrokinetic potentials in the range from –35 to –25 mV, which indicates their moderate stability of the studied samples with respect to agglomeration

and opportunity of the use of separate silicon particles-agents in biological tissues either in a short time after manufacture (no more than weeks), or after ultrasonication in the case of long-term storage.

3.3.2. Analysis of scattering and absorption coefficients spectra. For the numerical analysis of the spectral characteristics of scattering and absorption of light in the visible and near-infrared ranges (400–1000 nm), a suspension was selected obtained by laser fragmentation of SiMPs with an initial mass concentration of 12.0 mg mL^{-1} in water for 40 min. The choice of a suspension with the highest possible initial concentration of the micropowder is determined by the requirement to obtain SiNP ensembles also with high concentrations exceeding 0.1 mg mL^{-1} in water, when both accurate spectrophotometric measurements and high contrast in the OCT technique are provided [11, 16, 25]. According to the performed approximations of the absorption and scattering spectra of this suspension, it was demonstrated that during the irradiation time of 40 min, not all SiMPs are fragmented into SiNPs: the mass concentration of particles smaller than 500 nm suitable for further use is close to 0.1 mg mL^{-1} after sedimentation of a large fraction of SiMPs not subjected to fragmentation, accounting the contribution of this fraction not subjected to sedimentation as a result of centrifugation (see Section 3.1 and Fig. 3b). In this connection, taking into account the overestimated mass yield of SiNPs as a product of fragmentation in the case of lower initial concentrations of micropowder (see Section 3.2), the spectrophotometric measurements for suspensions with a known lower yield of SiNPs in the frames of this study seem to be of little significance from a practical point of view.

Figure 8 shows the spectra of the reconstructed values of the scattering and absorption coefficients, μ_s and μ_a, and the anisotropy factor g for the selected suspension of SiNPs. The scattering and absorption spectra calculated using the Mie formulae based on the size distribution of SiNPs (in accordance with Fig. 3e), as well as for the same distribution of SiNPs supplemented with a fraction of silicon spheres of 5 μm in diameter are shown in the same figure. The concentration of the latter was selected to ensure the best agreement between the model and measured spectra. The second approximation parameter was the total concentration of SiNPs and SiMPs in the studied suspension, which allowed one to estimate the mass yield of SiNPs during laser fragmentation.

The measured spectra exhibit features that are explained both by the optical properties of crystalline silicon and by the size distribution of particles in the suspension. The monotonic decrease in the reconstructed values of μ_a from 0.98 to 0.16 mm^{-1} (Fig. 8a) with increasing wavelength is explained by the similar behaviour of the absorption coefficient of crystalline silicon [53]. The presence of a μ_s maximum at 670 nm and high values of g in the range 0.50–0.62 (Fig. 8b) are explained by the typical features of Mie scattering for relatively large SiNPs [54] with average size of 147 nm, which is only 2.7–6.8 times smaller than the wavelengths from the considered spectral range. It is important to note that the reconstructed values of μ_s exceed 2 mm^{-1} as well as the typical values of μ_a (Fig. 8a), which indicates the potentials for using the fabricated SiNP suspensions for contrasting in such techniques as OCT due to high light scattering at depths of about 1 mm in the diagnostic window of transparency of biological tissues given a relatively small absorption of silicon.

At the same time, Fig. 8 shows that a suspension consisting only of SiNPs with a given size distribution only (Fig. 3e)

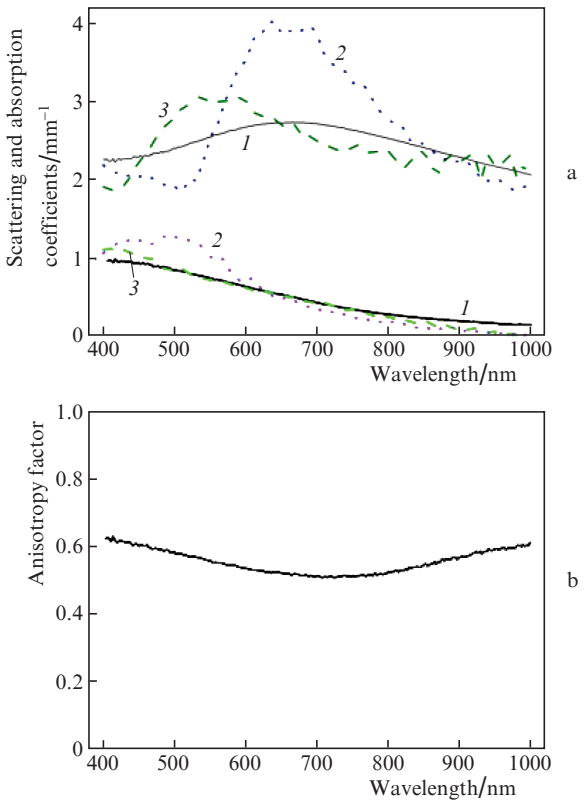

Figure 8. (a) Spectra of scattering (μ_s, upper group of curves) and absorption (μ_a, lower group of curves) coefficients reconstructed from spectrophotometric data for a suspension of silicon particles subjected to laser fragmentation of the initial powder of microcrystalline silicon with a mass concentration of 12.0 mg mL^{-1} (*1*) in water for 40 min, as well as the corresponding spectra calculated by the Mie theory without (*2*) (SiNPs) and with (*3*) (SiNPs + SiMPs) account for the fraction of spherical silicon microparticles with a diameter of 5 μm. (b) Spectrum of the anisotropy factor g reconstructed from spectrophotometric data for the studied suspension.

does not provide a good agreement between the calculated and measured spectra shapes: the decay rates (the wavelength derivative) of the scattering and absorption coefficients of the calculated dependences exceeds those for the measured spectra in the long-wavelength region. Taking into account the 0.1% (in terms of the number of particles) fraction of silicon microspheres with a diameter of 5 μm in calculations using the Mie formulae allows one to obtain the shape of the calculated spectra that most closely matches the measured dependences. The best quantitative agreement between the spectra were obtained for a total mass concentration of a suspension of SiNPs and SiMPs equal to 5 mg mL^{-1}. Note that these parameters (percentage of microspheres and mass concentration) are sufficient for correct approximation of the presented dependences of scattering and absorption without introducing other additional parameters.

Based on the parameters of the approximation, the contribution of the fraction of small nanoparticles (with a diameter of less than 500 nm) was calculated: small nanoparticles are more than 99% in number, but only about 2.4% in mass, which, for the total mass of a suspension of SiNPs and SiMPs, corresponds to the value of the mass of this fractions 0.12 mL. This value is significantly lower than the maximum possible mass of the melt of 5.2 mg mL^{-1} obtained from the calculations described in Section 3.2. On the one hand, there is no

obvious contradiction, since the theoretical calculations give the estimate of the maximum possible melt mass for the applied laser fragmentation technology, and according to the SEM results, even after centrifugation, a fraction of SiMPs that have not undergone fragmentation is noticeable (Fig. 2b). On the other hand, the conducted study shows for suspensions with initial mass concentrations exceeding 5 mg mL^{-1} that tight focusing of the laser beam in a turbid medium is not always achievable and is not always required to ensure the process of laser fragmentation. In this connection, it seems possible to fabricate SiNPs using the described technology employing lenses with a larger focal length compared to the one used in the study (80 mm), which will provide a more uniform heat distribution in the beam propagation region. An additional increase in the mass of molten silicon can also be achieved both by using lasers with higher energies and pulse repetition rates, and by forced mixing of microparticles during irradiation.

The spectrophotometry measurements of the selected suspensions have shown that for the fabricated SiNPs in the given concentration after filtering, the produced suspension using membrane filters has potential in further experiments with biotissues and their phantoms, in particular, as contrasting agents for OCT technique. Relatively high absorption coefficients of the produced suspension are comparable with the typical absorption coefficients of biological tissue in the considered wavelength range, which also indicates their prospects as absorbing contrast agents.

4. Conclusions

We have shown that upon irradiation of an aqueous suspension of SiMPs with mass concentrations in the range of 0.5–12 mg mL^{-1} by picosecond laser pulses at a wavelength of 1064 nm, fragmentation of these microparticles occurs, leading to the formation of nanoparticles with an average size in the range of 111–165 nm and size dispersion in the range of 49–76 nm. The size distributions of the fragmented SiNPs depend both on the time of exposure to laser pulses and on the SiMP concentration in the initial suspension. Numerical simulation of the process of interaction of focused laser radiation with fragmented particles indicates that silicon is heated to temperatures above the melting temperature, and the SiNP formation occurs in the focal region around the laser beam axis in the suspension volume or in the sub-surface region in the cases of low and high initial mass concentrations of SiMPs, respectively.

The results of spectrophotometric measurements of the fabricated SiNPs suspensions are in good agreement with the estimates of absorption and scattering spectra according to the Mie theory for the size distributions obtained from scanning electron microscopy data analysis. SiNPs after additional filtering out the microparticles that have not undergone fragmentation are of interest for further experiments with biotissues or their phantoms as effective light scattering and absorbing contrasting agents in the diagnostic/transparency window of biotissues. In the future, the number of unfragmented SiMPs can be reduced by using laser sources with higher pulse energies and pulse repetition rates. However, most likely, the former case will require the fragmentation regime variation by loosing the beam focusing, while in the latter one the pulse delay reduction will require account for an additional heat during this period of time. Both cases will require an improvement of the model proposed in this study explaining the morphology of the silicon nanoparticles fabricated in the experiments.

Acknowledgements. This work was supported by the Russian Science Foundation (Grant No. 19-12-00192).

References

1. Ksenofontova O.I., Vasin A.V., Egorov V.V., Bobyl A.V., Soldatenkov F.Yu., Terukov E.I., Ulin V.P., Ulin N.V., Kiselev O.I. *Tech. Phys*., **59**, 66 (2014) [*Zh. Tekh. Fiz*., **84** (1) 67 (2014)].
2. Stojanovic V., Cunin F., Durand J.O., Garcia M., Gary-Bobo M. *J. Mater. Chem. B*, **4**, 7050 (2016).
3. Park J.-H., Gu L., von Maltzahn G., Ruoslahti E., Bhatia S.N., Sailor M.J. *Nature Mater*., **8** (4), 331 (2009).
4. Sviridov A.P., Osminkina L.A., Kharin A.Yu., Gongalsky M.B., Kargina J.V., Kudryavtsev A.A., Bezsudnova Yu.I., Perova T.S., Geloen A., Lysenko V., Timoshenko V.Yu. *Nanotechnology*, **28**, 105102 (2017).
5. Chaix A., Cheikh K.E., Bouffard E., Maynadier M., Aggad D., Stojanovic V., Knezevic N., Garcia M., Maillard P., Morère A., Gary-Bobo M., Raehm L., Richeter S., Durand J.-O., Cunin F. *J. Mater. Chem. B*, **4**, 3639 (2016).
6. Xiao L., Gu L., Howell S.B., Sailor M.J. *ACS Nano*, **5** (5), 3651 (2011).
7. Secret E., Maynadier M., Gallud A., Chaix A., Bouffard E., Gary-Bobo M., Marcotte N., Mongin O., Cheikh K.E., Hugues V., Auffan M., Frochot C., Morère A., Maillard P., Blanchard-Desce M., Sailor M.J., Garcia M., Durand J.-O., Cunin F. *Adv. Mater*., **26**, 7643 (2014).
8. Sviridov A.P., Andreev V.G., Ivanova E.M., Osminkina L.A., Tamarov K.P., Timoshenko V.Yu. *Appl. Phys. Lett*., **103**, 193110 (2013).
9. Tamarov K.P., Osminkina L.A., Zinovyev S.V., Maximova K.A., Kargina Ju.V., Gongalsky M.B., Ryabchikov Yu., Al-Kattan A., Sviridov A.P., Sentis M., Ivanov A.V., Nikiforov V.N., Kabashin A.V., Timoshenko V.Yu. *Sci. Rep*., **4**, 7034 (2014).
10. Hong C., Lee J., Zheng H., Hong S.-S., Lee C. *Nanoscale Res. Lett*., **6**, 321 (2011).
11. Zabotnov S.V., Kashaev F.V., Shuleiko D.V., Gongalsky M.B., Golovan L.A., Kashkarov P.K., Loginova D.A., Agrba P.D., Sergeeva E.A., Kirillin M.Yu. *Quantum Electron*., **47** (7), 638 (2017) [*Kvantovaya Elektron*., **47** (7), 638 (2017)].
12. Tolstik E., Osminkina L.A., Matthäus C., Burkhardt M., Tsurikov K.E., Natashina U.A., Timoshenko V.Yu., Heintzmann R., Popp J., Sivakov V. *Nanomed. Nanotechnol. Biol. Med*., **12**, 1931 (2016).
13. Osminkina L.A., Sivakov V.A., Mysov G.A., Georgobiani V.A., Natashina U.A., Talkenberg F., Solovyev V.V., Kudryavtsev A.A., Timoshenko V.Yu. *Nanoscale Res. Lett*., **9**, 463 (2014).
14. Baati T., Al-Kattan A., Esteve M.-A., Njim L., Ryabchikov Yu., Chaspoul F., Hammami M., Sentis M., Kabashin A.V., Braguer D. *Sci. Rep*., **6**, 25400 (2016).
15. Al-Kattan A., Ryabchikov Yu.V., Baati T., Chirvony V., Sánchez-Royo J.F., Sentis M., Braguer D., Timoshenko V.Yu., Estève M.-A., Kabashin A.V. *J. Mater. Chem. B*, **4**, 7852 (2016).
16. Zabotnov S.V., Kurakina D.A., Kashaev F.V., Skobelkina A.V., Kolchin A.V., Kaminskaya T.P., Khilov A.V., Agrba P.D., Sergeeva E.A., Kashkarov P.K., Kirillin M.Yu., Golovan L.A. *Quantum Electron*., **50** (1), 69 (2020) [*Kvantovaya Elektron*., **50** (1), 69 (2020)].
17. Gongalsky M.B., Osminkina L.A., Pereira A., Manankov A.A., Fedorenko A.A., Vasiliev A.N., Solovyev V.V., Kudryavtsev A.A., Sentis M., Kabashin A.V., Timoshenko V.Yu. *Sci. Rep*., **6**, 24732 (2016).
18. Kirillin M.Yu., Sergeeva E.A., Agrba P.D., Krainov A.D., Ezhov A.A., Shuleiko D.V., Kashkarov P.K., Zabotnov S.V. *Laser Phys*., **25** (7), 075604 (2015).
19. Rioux D., Laferriere M., Douplik A., Shah D., Lilge L., Kabashin A.V., Meunier M.M. *J. Biomed. Opt*., **142**, 021010 (2009).
20. Al-Kattan A., Nirwan V.P., Popov A., Ryabchikov Yu.V., Tselikov G., Sentis M., Fahmi A., Kabashin A.V. *Int. J. Mol. Sci*., **19**, 1563 (2018).

21. Oleshchenko V.A., Kharin A.Yu., Alykova A.F., Karpukhina O.V., Karpov N.V., Popov A.A., Bezotosnyi V.V., Klimentov S.M., Zavestovskaya I.N., Kabashin A.V., Timoshenko V.Yu. *Appl. Surf. Sci*., **516**, 145661 (2020).
22. Sokolovskaya O.I., Zabotnov S.V., Golovan L.A., Kashkarov P.K., Kurakina D.A., Sergeeva E.A., Kirillin M.Yu. *Quantum Electron.*, **51** (1), 64 (2021) [*Kvantovaya Elektron*., **51** (1), 64 (2021)].
23. Skobelkina A.V., Kashaev F.V., Kolchin A.V., Shuleiko D.V., Kaminskaya T.P., Presnov D.E., Golovan L.A., Kashkarov P.K. *Tech. Phys. Lett*., **46**, 687 (2020) [*Pis'ma Zh. Tekh. Fiz*., **46** (14), 13 (2020)].
24. Zabotnov S.V., Skobelkina A.V., Kashaev F.V., Kolchin A.V., Popov V.V., Presnov D.E., Sergeeva E.A., Kirillin M.Yu., Golovan L.A. *Solid State Phenomena*, **312**, 200 (2020).
25. Zabotnov S.V., Skobelkina A.V., Sergeeva E.A., Kurakina D.A., Khilov A.V., Kashaev F.V., Kaminskaya T.P., Presnov D.E., Agrba P.D., Shuleiko D.V., Kashkarov P.K., Golovan L.A., Kirillin M.Yu. *Sensors*, **20**, 4874 (2020).
26. Ryabchikov Yu.V. *Phys. Status Solidi A*, **216** (2), 1800685 (2019).
27. Blandin P., Maximova K.A., Gongalsky M.B., Sanchez-Royo J.F., Chirvony V.S., Sentis M., Timoshenko V.Yu., Kabashin A.V. *J. Mater. Chem. B*, **1** (19), 2489 (2013).
28. Zabotnov S.V., Kolchin A.V., Kashaev F.V., Skobelkina A.V., Nesterov V.Yu., Presnov D.E., Golovan L.A., Kashkarov P.K. *Tech. Phys. Lett*., **45**, 1085 (2019) [*Pis'ma Zh. Tekh. Fiz*., **45** (21), 22 (2019)].
29. Ryabchikov Yu.V. *J. Nanopart. Res*., **21**, 85 (2019).
30. Libenson M.N. *Lazerno-indutsirovannye opticheskie i termicheskie protsessy v kondensirovannykh sredakh i ikh vzaimnoe vliyanie* (Laser-Induced Optical and Thermal Processes in Condensed Media and Their Mutual Effect) (St. Petersburg: Nauka, 2007).
31. Taylor L.L., Scott R.E., Qiao J. *Opt. Mater. Express*, **8**, 648 (2018).
32. Wang L., Jacques S.L., Zheng L. *Comput. Meth. Programs Biomed*., **47** (2), 131 (1995).
33. Loginova D.A., Sergeeva E.A., Fiks I.I., Kirillin M.Yu. *J. Biomed. Photon. Eng*., **3** (1), 010303 (2017).
34. Manuchehrabadi N., Chen Y., LeBrun A., Ma R., Zhu L. *J. Biomech. Eng*., **135** (12), 121007 (2013).
35. Box G.E.P., Muller M.E. *Ann. Math. Statist*., **29**, 610 (1958).
36. Ohmura E., in *Heat Transfer-Engineering Applications* (London: IntechOpen, 2011).
37. Aspnes D.E., Studna A.A. *Phys. Rev. B*, **27**, 985 (1983).
38. Jellison G.E. Jr, Burke H.H. *J. Appl. Phys*., **60**, 841 (1986).
39. Fuchs M.S.K. *J. Phys.:Condens. Matter*, **12**, 4341 (2000).
40. Segelstein D.J. PhD Diss. (Kansas City: University of Missouri, 1981).
41. Bohren C.F., Huffman D.R. *Absorption and Scattering of Light by Small Particles* (New York: John Wiley & Sons, 2008).
42. Born M., Wolf E. *Principles of Optics* (Oxford: Pergamon Press, 1969).
43. Golovan L.A., Zabotnov S.V., Timoshenko V.Yu., Kashkarov P.K. *Semiconductors*, **43**, 218 (2009) [*Fiz. Tekh. Poluprovodn*., **43** (2), 230 (2009)].
44. Henyey L.G., Greenstein J.L. *Astrophys. J*., **93**, 70 (1941).
45. Wood R.F., Geist G.A. *Phys. Rev. B*, **34** (4), 2606 (1986).
46. Hale G.M., Querry M.R. *Appl. Opt*., **12**, 555 (1973).
47. Kirillin M.Yu., Shirmanova M.V., Sirotkina M.A., Bugrova M., Khlebtsov B.N., Zagainova E.V. *J. Biomed. Opt*., **14** (2), 21017 (2009).
48. Slade A.B., Aguilar G. *Comput. Meth. Programs Biomed*., **118** (2), 234 (2015).
49. Knunyantz I.L. *Khimicheskaya entsiklopediya* (Chemical Encyclopaedia) (Moscow: Sovetskaya Entsiklopediya, 1990) Vol. 2.
50. Huang H., Zhigilei L.V. *J. Phys. Chem. C*, **125**, 13413 (2021).
51. Hull R. *Properties of Crystalline Silicon* (London: INSPEC, 1999).
52. Akhmanov S.A., Nikitin S.Yu. *Physical Optics* (Oxford: Clarendon Press, 1997).
53. Philipp H.R., Taft E.A. *Phys. Rev*., **120** (1), 37 (1960).
54. Matveev A.N. *Optika* (Optics) (Moscow: Vysshaya Shkola, 1988).